OPEN ACCESS



Observational Constraints on Direct Electron Heating in the Hot Accretion Flows in Sgr A* and M87*

Fu-Guo Xie ¹, Ramesh Narayan ^{2,3}, and Feng Yuan ^{1,4} ¹ Key Laboratory for Research in Galaxies and Cosmology, Shanghai Astronomical Observatory, Chinese Academy of Sciences, 80 Nandan Road, Shanghai 200030, People's Republic of China

² Center for Astrophysics, Harvard & Smithsonian, 60 Garden Street, Cambridge, MA 02138, USA Black Hole Initiative at Harvard University, 20 Garden Street, Cambridge, MA 02138, USA ⁴ University of Chinese Academy of Sciences, No. 19A Yuquan Road, Beijing 100049, People's Republic of China Received 2022 October 6; revised 2022 November 14; accepted 2022 November 21; published 2022 December 30

Abstract

An important parameter in the theory of hot accretion flows around black holes is δ , which describes the fraction of "viscously" dissipated energy in the accretion flow that goes directly into heating electrons. For a given mass accretion rate, the radiative efficiency of a hot accretion flow is determined by δ . Unfortunately, the value of δ is hard to determine from first principles. The recent Event Horizon Telescope Collaboration (EHTC) results on M87* and Sgr A* provide us with a different way of constraining δ . By combining the mass accretion rates in M87* and Sgr A* estimated by the EHTC with the measured bolometric luminosities of the two sources, we derive good constraints on the radiative efficiencies of the respective accretion flows. In parallel, we use a theoretical model of hot magnetically arrested disks (MADs) to calculate the expected radiative efficiency as a function of δ (and accretion rate). By comparing the EHTC-derived radiative efficiencies with the theoretical results from MAD models, we find that Sgr A* requires $\delta \gtrsim 0.3$. A similar comparison in the case of M87* gives inconclusive results as there is still a large uncertainty in the accretion rate in this source.

Unified Astronomy Thesaurus concepts: Accretion (14); Low-luminosity active galactic nuclei (2033); Supermassive black holes (1663); Galactic center (565)

1. Introduction

Accretion flows around black holes (BHs) can be divided into two types: hot accretion flows, which occur at accretion rates below about 1% of Eddington (Narayan & Yi 1994, 1995; Abramowicz et al. 1995, see Yuan & Narayan 2014 for a review),⁵ and cold accretion disks, which are found at accretion rates closer to Eddington (Novikov & Thorne 1973; Shakura & Sunyaev 1973; Pringle 1981). Most supermassive BHs in the nearby universe have low accretion rates and are believed to have hot accretion flows (Ho 2008).

The plasma in a hot accretion flow has two temperatures (Shapiro et al. 1976), with electrons and ions having different temperatures. Hence the two species need to be treated with separate energy equations (Narayan & Yi 1995; Yuan & Narayan 2014). The energy equation of electrons takes the form

$$\rho V_r \left(\frac{de_e}{dR} - \frac{p_e}{\rho^2} \frac{d\rho}{dR} \right) = q_{ie} + \delta q_{vis} - q^-, \tag{1}$$

where ρ is the gas density; V_r is the radial velocity; R is the radius; $e_{\rm e}$ and $p_{\rm e}$ are, respectively, the specific internal energy

Original content from this work may be used under the terms of the Creative Commons Attribution 4.0 licence. Any further distribution of this work must maintain attribution to the author(s) and the title of the work, journal citation and DOI.

and pressure of electrons; and q^- is the radiative cooling rate per unit volume. The first two terms in the right-hand side of Equation (1) correspond to two different mechanisms by which electrons are heated. One mechanism is via Coulomb collisions between ions and electrons, denoted by q_{ie} ; the other is through direct "viscous heating," which is a catchall term describing several physical dissipation processes in the plasma as we explain in the next paragraph. We assume that, out of the total viscous heating rate per unit volume q_{vis} , a fraction δq_{vis} heats the electrons, and the rest $(1 - \delta)q_{\text{vis}}$ heats the ions. Since almost all the radiation of the accretion flow is emitted by electrons; therefore, when other model parameters such as the mass accretion rate are given, the value of δ determines the radiative efficiency ϵ of the accretion flow, which we define as

$$\epsilon = \frac{L_{\text{bol}}}{\dot{M}_{\text{BH}}c^2} = 10\% \, \frac{L_{\text{bol}}/L_{\text{Edd}}}{\dot{M}_{\text{BH}}/\dot{M}_{\text{Edd}}}.\tag{2}$$

Here L_{bol} is the bolometric luminosity of the accretion flow, and $\dot{M}_{\rm BH}$ is the mass accretion rate at the BH horizon. In the second expression, the luminosity and the accretion rate are normalized to, respectively, the Eddington luminosity $L_{\rm Edd}$ and the Eddington accretion rate $\dot{M}_{\rm Edd} = L_{\rm Edd}/(0.1c^2) = 2.21 \times$ $10^{-2} (M_{\rm BH}/10^6 M_{\odot}) M_{\odot} {\rm yr}^{-1}$.

The viscous heating rate of electrons $\delta q_{
m vis}$ includes several microphysical processes. Many attempts have been made to estimate δ from first-principle calculations of these processes, including magnetic reconnection (Bisnovatyi-Kogan & Lovelace 1997; Quataert & Gruzinov 1999; Ding et al. 2010; Hoshino 2012, 2013; Numata & Loureiro 2015; Sironi & Narayan 2015; Rowan et al. 2017, 2019; Ball et al. 2018), magnetohydrodynamic (MHD) turbulence (Quataert 1998;

Note that the 1% limit quoted here is a typical value for low-luminosity active galactic nuclei (Ho 2008). In the case of BH X-ray binaries in the hard state (Remillard & McClintock 2006; Done et al. 2007), where again hot accretion flows are present (Esin et al. 1997), the luminosity can reach much higher values, \gtrsim 10%–20% of the Eddington luminosity $L_{\rm Edd}$ (e.g., Dunn et al. 2010). Here $L_{\rm Edd}=4\pi Gcm_p M_{\rm BH}/\sigma_T=1.26\times 10^{44}~(M_{\rm BH}/10^6 M_{\odot})~{\rm erg~s}^{-1}$ for accretion onto a BH with mass $M_{\rm BH}$.

Blackman 1999; Quataert & Gruzinov 1999; Medvedev 2000; Lehe et al. 2009; Howes 2010; Ressler et al. 2015; Ryan et al. 2017), dissipation of pressure anisotropy in a collisionless plasma (Sharma et al. 2007), or low Mach number shocks (Guo et al. 2017, 2018). Unfortunately, there is no consensus, and the value of δ remains poorly determined.

Yuan et al. (2003) considered an alternative approach to constrain the value of δ . By calculating the dynamics and radiation of the accretion flow using a height-integrated model and comparing the results with observations of the supermassive BH Sagittarius A^* (Sgr A^*) at the center of our Galaxy, they estimated $\delta \sim 0.5$.

In this work, we follow the approach of Yuan et al. (2003) and estimate the value of δ using new and updated observational data and a more modern theoretical model. Specifically, we make use of results from the Event Horizon Telescope (EHT), an Earth-size submillimeter radio interferometer, which has recently obtained 230 GHz images of the innermost horizon-scale regions of the low-luminosity supermassive BHs, M87* (Event Horizon Telescope Collaboration et al. 2019, 2021), and Sgr A* (Event Horizon Telescope Collaboration et al. 2022a). Key results from the work of the EHT Collaboration (EHTC) are estimates of the mass accretion rates $\dot{M}_{\rm BH}$ for the two sources to within a factor of several; see Section 2 below. By combining these estimates with a reliable measurement of the bolometric luminosities of the sources from their broadband spectra, we are able to evaluate the radiative efficiencies ϵ (see Equation (2)) of the two sources. We compare these measurements with the predictions of the model described in Xie & Zdziarski (2019) and thereby evaluate the value of δ .

Before going into detail, we briefly introduce additional background information on hot accretion flows. In the past decade or two, it has become clear that the degree of magnetization of the accretion flow plays an important role in the dynamics and observational characteristics of hot accretion flows. Broadly, one distinguishes between two kinds of models. One has relatively weak magnetic fields and is referred to as the standard and normal evolution (SANE) model, while the other has the maximum saturated level of the magnetic field and is called the magnetically arrested disk (MAD) model (Bisnovatyi-Kogan & Ruzmaikin 1974, 1976; Igumenshchev et al. 2003; Narayan et al. 2003; Tchekhovskoy et al. 2011; McKinney et al. 2012; Liska et al. 2020). The dynamical differences between the SANE and MAD models are investigated in detail in Narayan et al. (2012; see also Begelman et al. 2022; Chatterjee & Narayan 2022).

The accumulation of a considerable quantity of poloidal magnetic flux around the BH in the MAD state has the attractive feature that it provides the ideal magnetic field configuration to launch a powerful relativistic jet (Tchekhovskoy et al. 2011; Liska et al. 2020; Narayan et al. 2022). Indeed, there is accumulating evidence that systems with strong relativistic jets are generally MADs, e.g., Zamaninasab et al. (2014), Ghisellini et al. (2014), and Zdziarski et al. (2015) for a sample of blazars. Meanwhile, the EHT has provided evidence that M87* and Sgr A* may also both be MADs (Event Horizon Telescope Collaboration et al. 2021, 2022a). The MAD nature of M87* has been confirmed by an analysis of the observed Faraday rotation measure (RM; Yuan et al. 2022). These results lead one to speculate that perhaps the MAD configuration is the inevitable

final state of most hot accretion flows in nature (e.g., Narayan et al. 2022).

The radiative properties of MAD flows are found to be fairly similar to those of SANE flows, except that, for a given accretion rate, MAD is brighter by about a factor of \sim 3 (Xie & Zdziarski 2019). This motivates us to use a model appropriate to MAD systems when attempting to estimate the electron heating parameter δ .

This paper is organized as follows. In Section 2, we provide the observational and modeling results for Sgr A* and M87*, with an emphasis on the accretion rate $\dot{M}_{\rm BH}$, the bolometric luminosity $L_{\rm bol}$, and the radiative efficiency ϵ . In Section 3, we present theoretical calculations of the radiative efficiency of MAD flows corresponding to different values of δ . We then compare these theoretical results with the values of ϵ inferred by the EHTC for Sgr A* and M87*, and we thereby constrain the value of δ . Section 4 is devoted to a brief summary.

2. Observational Constraints on the Radiative Efficiency

Both M87* and Sgr A* are low-luminosity systems with hot accretion flows. They are the main targets of the EHT project. Below we provide basic properties of the two sources and derive their radiative efficiencies.

2.1. M87*

 $M87^*$ is located at a distance of $d = 16.9 \,\mathrm{Mpc}$, and the BH mass is measured to be $M_{\rm BH} = 6.2 \times 10^9 M_{\odot}$ (Gebhardt et al. 2011; Event Horizon Telescope Collaboration et al. 2019). By comparing the values of four physical quantities obtained from theoretical predictions and those derived from the reconstructed EHT image of M87* and the Atacama Large Millimeter/ submillimeter Array (ALMA)-only measurements, the EHTC concluded that the accretion flow in M87* is very likely in an MAD state (Event Horizon Telescope Collaboration et al. 2021). This result has been confirmed recently by Yuan et al. (2022) by comparing the predicted Faraday RM in M87* with that measured along the jet. The advantage of the latter work is that it does not suffer from uncertainties in the electron temperature and the contribution of nonthermal electrons in the accretion flow, which are a challenge for the EHTC analysis. The spin of the BH in M87* is hard to determine (Event Horizon Telescope Collaboration et al. 2021), but some recent works have begun to constrain its value by comparing observed images of the M87* jet with theoretical predictions (Cruz-Osorio et al. 2022; Yang et al. 2022).

Broadband quasi-simultaneous observations of M87* indicate that the turnover frequency of the submillimeter bump in the νL_{ν} plot is located at ~230 GHz (Algaba et al. 2021; see also Hada et al. 2011) and that the bolometric luminosity is approximately $L_{\rm bol} \approx 8.5 \times 10^{41} \, {\rm erg \ s^{-1}} \approx 1.1 \times 10^{-6} \, L_{\rm Edd}$. In estimating the bolometric luminosity, we only include nuclear emission; see Figure 16 and Model 1a of Algaba et al. (2021). We adopt a 20% uncertainty in $L_{\rm bol}$.

The second piece of information we need is the mass accretion rate in M87*. From the RM measurements of the nucleus of M87* at submillimeter wavelengths and using an argument previously developed by Agol (2000) and Quataert & Gruzinov (2000), Kuo et al. (2014) derived an upper limit on

⁶ Note that Prieto et al. (2016) derived a larger value of the bolometric luminosity: $L_{\rm bol} \approx 3 \times 10^{42} \, {\rm erg \, s^{-1}}$. The main difference from Algaba et al. (2021) is the treatment of data in optical/UV.

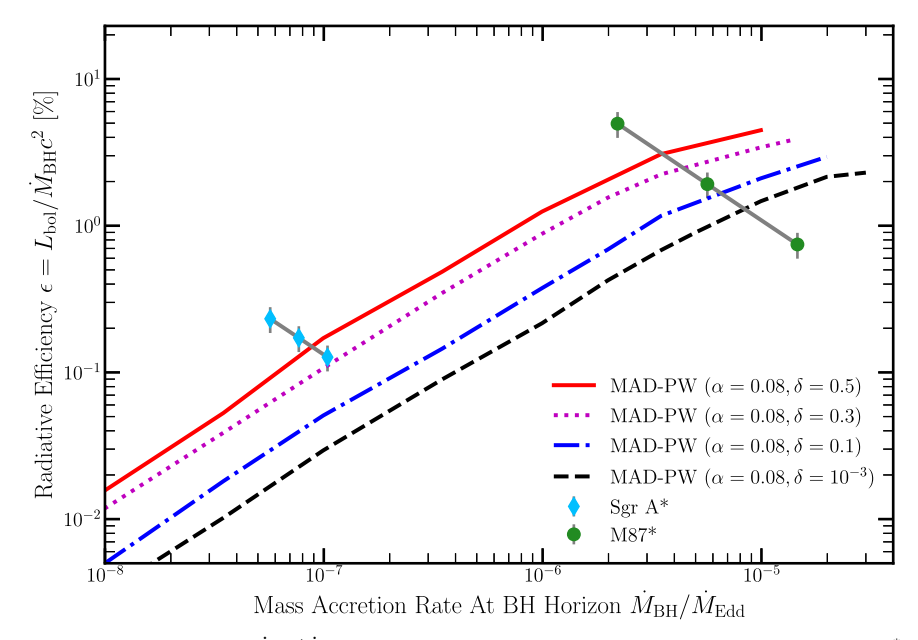


Figure 1. Radiative efficiencies ϵ vs. mass accretion rates $\dot{M}_{\rm BH}/\dot{M}_{\rm Edd}$ of MAD systems. Observational constraints obtained from M87* and Sgr A* (see Section 2) are shown, respectively, by the green circles and cyan diamonds, connected by gray solid curves. The colored lines correspond to numerical results from a theoretical, pseudo-Newtonian (Paczyński–Wiita) potential version of an MAD. From top to bottom, the curves correspond to different values of the electron heating fraction: $\delta = 0.5$ (red solid), 0.3 (purple dotted), 0.1 (blue dotted–dashed), and 10^{-3} (black dashed). For a given δ , the radiative efficiency in the models scales as $\epsilon \propto \dot{M}_{\rm BH}^{0.92}$. All calculations use a viscosity parameter $\alpha = 0.08$ (see Section 3.2).

the accretion rate: $\dot{M}_{\rm BH} < 9.2 \times 10^{-4} M_{\odot} \ \rm yr^{-1}$. EHT observations now allow a more careful analysis.

The one-zone model discussed in Event Horizon Telescope Collaboration et al. (2019) provides a first approximate estimate of $\dot{M}_{\rm BH}$. The emission size (radius R) of the accretion flow is directly measured from the diameter of the ring in the EHT image. Combining this with the submillimeter flux, brightness temperature, and synchrotron peak frequency, one estimates the density as well as the magnetic field strength at radius R. This, along with an estimate of the radial velocity of the gas, then gives an approximate estimate of the mass accretion rate $\dot{M}_{\rm BH} \sim 25 \times 10^{-4} M_{\odot} \ \rm yr^{-1}$.

The above estimate is further refined in Event Horizon Telescope Collaboration et al. (2021), where EHT polarimetric data are included as important additional constraints, and elaborate theoretical models are developed based on GRMHD simulations. The conclusion of this work is that the mass accretion rate near the BH horizon in M87* lies in the range $\dot{M}_{\rm BH} \approx (3-20) \times 10^{-4} M_{\odot} \, {\rm yr}^{-1}$ (Event Horizon Telescope Collaboration et al. 2021), or equivalently, $\dot{M}_{\rm BH}/\dot{M}_{\rm Edd} = (2.2-15) \times 10^{-6}$. This is the range we use in the present work. Note that the EHT result is generally consistent with the initial estimate of Kuo et al. (2014) based on polarimetric data.

Combining the estimates of the bolometric luminosity and mass accretion rate discussed above, we derive the radiative efficiency ϵ (see Equation (2)) of M87* to be

$$7.5 \times 10^{-3} \lesssim \epsilon \lesssim 5.0 \times 10^{-2},$$
 (3)

where the range is driven almost entirely by the uncertainty in $\dot{M}_{\rm BH}$. The two extreme values of the radiative efficiency and their geometric mean are shown in Figure 1 as green filled circles. The gray solid curve connecting the three points represents the allowed combinations of ϵ and $\dot{M}_{\rm BH}$.

We note that the above estimates of $\dot{M}_{\rm BH}$ are based on the assumption that the electrons have a thermal distribution. Although electrons and ions in a hot accretion flow are poorly

coupled via Coulomb collisions, electron–electron collisions are more effective and will maintain a thermal distribution, at least for moderately large accretion rates. Mahadevan & Quataert (1997) have shown that synchrotron self-absorption couples electrons efficiently at even lower accretion rates. They estimate that electrons remain thermal so long as

$$\frac{\dot{M}_{\rm BH}}{\dot{M}_{\rm Edd}} > 10^{-4} \, \frac{\alpha^2}{\Theta_e},\tag{4}$$

where $\alpha \sim 0.1$ is the effective viscosity parameter of the accretion flow (Shakura & Sunyaev 1973; see also Section 3.2) and $\Theta_e = kT_e/m_ec^2 \sim$ few is the dimensionless electron temperature in the hot accretion flow. M87* satisfies the above constraint, so the thermal assumption is probably reasonable.

A weak nonthermal tail in the electron distribution is partially equivalent to a thermal model with a higher electron temperature (e.g., Event Horizon Telescope Collaboration et al. 2022a). However, models that include a significant nonthermal component are quite different from thermal models (Event Horizon Telescope Collaboration et al. 2019). For a given radio flux, including nonthermal electrons generally leads to a lower estimate for the accretion rate (lower optical depth) and thus to a larger radiative efficiency.

2.2.
$$Sgr A^*$$

The second object we consider is Sgr A*. It is at a distance of d=8.13 kpc and has a BH mass of $M_{\rm BH}=4.14\times10^6M_{\odot}$ (both are average values as adopted in Event Horizon Telescope Collaboration et al. 2022a). According to the EHT work, the accretion flow in Sgr A* is probably in an MAD state; specifically, Event Horizon Telescope Collaboration et al. (2022a) showed that MAD models are more consistent with observational constraints in Sgr A* compared to SANE models, although the favored models are generally too variable compared to observations (a presently unsolved problem).

The spectrum of Sgr A* peaks at the submillimeter wave band (von Fellenberg et al. 2018; Bower et al. 2019; Event Horizon Telescope Collaboration et al. 2022b), and the luminosity of this submillimeter bump is $\approx 5.0 \times 10^{35}\,\mathrm{erg\,s^{-1}}$ (see Bower et al. 2019; Event Horizon Telescope Collaboration et al. 2022b). The near-infrared emission (Witzel et al. 2018), which also originates from the inner accretion flow, should be included when we estimate the bolometric luminosity. Adopting a spectrum that takes the form of a power law with exponential cutoff near 10¹³ Hz (i.e., $F_{\nu} \propto \nu^{\alpha} \exp(-\nu/10^{13} \text{ Hz})$; Bower et al. 2019), we empirically derive a luminosity of $\approx 1.9 \times 10^{35} \text{ erg s}^{-1}$ for the infrared emission (we take the 50th percentile of Witzel et al. 2018 as representative; see their Figure 19). Combining the submillimeter and infrared contributions, the bolometric luminosity of Sgr A* is estimated to be $L_{\rm bol} \approx 6.9 \times 10^{35} \, {\rm erg \ s^{-1}} = 1.5 \times 10^{-9} \, L_{\rm Edd}$. This model-independent measurement of $L_{\rm bol}$ agrees with values derived from MAD models (Event Horizon Telescope Collaboration et al. 2022a), which are in the range $L_{\rm bol} = (6.8-9.2) \times 10^{35} \, {\rm erg \ s^{-1}}$. The X-ray emission of Sgr A* during the quiescent state mainly originates from the region $R > 10^4 R_g$ (here $R_g = GM_{\rm BH}/c^2$ is the gravitational radius of the BH). Detailed analysis of high-resolution Chandra observations indicates that nuclear $(R < 10^3 R_g)$ X-ray emission has only $\nu L_{\nu} \approx 1.0 \times 10^{32} \, \mathrm{erg \, s^{-1}}$ at 5 keV (Roberts et al. 2017). It is 3 orders of magnitude fainter than the submillimeter bump; thus, we ignore this contribution. For the uncertainty in our L_{bol} measurement of Sgr A*, we again assume that it is 20% of L_{bol} .

Early hot accretion flow models of Sgr A* invoked mass accretion rates at the BH comparable to the Bondi accretion rate, but such large rates were thrown into doubt when linear polarization was reported in Sgr A* at millimeter wavelengths by Aitken et al. (2000; later confirmed by Bower et al. 2003). In two influential papers, Agol (2000) argued that this detection implied that the RM must be low, and hence $\dot{M}_{\rm BH}$ must be $<10^{-8}M_{\odot}~\rm yr^{-1}$, while Quataert & Gruzinov (2000) used a similar argument to estimate $\dot{M}_{\rm BH}\approx 10^{-8}M_{\odot}~\rm yr^{-1}$.

Recently, Event Horizon Telescope Collaboration et al. (2022a; see references therein for earlier theoretical/observational studies) combined observational constraints from the 230 GHz EHT image of Sgr A* with detailed simulations-based theoretical models to come up with a tight constraint on the mass accretion rate in Sgr A*: $\dot{M}_{\rm BH} = (5.2-9.5) \times 10^{-9} \, M_{\odot} \, \rm yr^{-1}$ or, equivalently, $\dot{M}_{\rm BH} / \dot{M}_{\rm Edd} = (5.7-10.4) \times 10^{-8}$. Although these models do not include any spatially resolved polarization constraints from the EHT (none have been published yet), the estimated $\dot{M}_{\rm BH}$ is perfectly consistent with the original estimates from Agol (2000), Quataert & Gruzinov (2000), and subsequent work following the same lines. We use the quoted EHT-derived range in the present work.

Using the above estimates of the bolometric luminosity and the mass accretion rate, we estimate the radiative efficiency ϵ of Sgr A* to be in the range

$$1.3 \times 10^{-3} \lesssim \epsilon \lesssim 2.3 \times 10^{-3}$$
. (5)

This range is shown in Figure 1 as cyan diamonds connected by a gray solid curve. The constraint on ϵ in the case of Sgr A* is much tighter than in M87*. This is because of the factor of <2 uncertainty in $\dot{M}_{\rm BH}$, which is perhaps a little optimistic. However, none of our conclusions will be affected even if we allow another factor of 2 uncertainty.

2.3. Comparing the Two Objects

The radiative efficiencies of M87* and Sgr A*, together with the large difference in their Eddington-scaled accretion rates, confirm an important theoretical prediction of hot accretion flow theory. All models, however much they may differ in physics details or parameter choices, agree that the radiative efficiency of hot accretion flows should decrease with decreasing Eddington-scaled mass accretion rate $\dot{M}_{\rm BH}/\dot{M}_{\rm Edd}$ (e.g., Narayan & Yi 1995; Narayan et al. 1999; Xie & Yuan 2012; Xie & Zdziarski 2019, and Figure 1 here). This is clearly borne out by the EHT-derived estimates for M87* and Sgr A*. However, due to the large uncertainty in $\dot{M}_{\rm BH}/\dot{M}_{\rm Edd}$ (especially the factor of ~7 uncertainty in the case of M87*), it is not possible to reliably estimate the slope of the $\epsilon-\dot{M}_{\rm BH}/\dot{M}_{\rm Edd}$ relation from current observational data.

3. Radiative Efficiency of the MAD Model

3.1. The MAD Model

In our numerical model of hot accretion flows in the MAD state, we assume for simplicity a nonspinning BH and adopt a pseudo-Newtonian Paczyński-Wiita gravitational potential (Paczyński & Wiita 1980) to mimic the potential of the BH. Since relativity is not explicitly taken into account in the dynamics of our model, the radial velocity can unphysically exceed the speed of light c near the BH horizon. To correct for this, we follow Xie et al. (2010) and interpret the velocity $V_{r,\mathrm{PW}}$ in our Paczyński-Wiita potential model as $\gamma V_{r,\mathrm{real}}$, where γ is the bulk Lorentz factor of the accreting gas and $V_{r,\mathrm{real}}$ is the corrected radial velocity.

The neglect of BH spin in the model is reasonable. Although the jet power depends sensitively on spin (e.g., Tchekhovskoy et al. 2010), the emission from the main body of the accretion flow has only a weak dependence. This is because, unlike the cold accretion disk model (Shakura & Sunyaev 1973) where the location of the disk's inner edge varies substantially with BH spin, a hot accretion flow extends down to the BH horizon $R_{\rm horizon}$, which is much less sensitive to BH spin. Dynamical properties of the flow outside $(3-5)R_{\rm horizon}$ are mostly unaffected by BH spin, while emission from regions inside of $\sim 2R_{\rm horizon}$ (e.g., radius of marginally bound orbit) is mostly beamed toward the BH and lost through the horizon.

The details of our MAD model and its radiation calculation can be found in Xie & Zdziarski (2019). Below we highlight the main points. Guided by numerical simulations, Xie & Zdziarski (2019) solve in cylindrical coordinates the heightintegrated equations of a steady MAD system, paying attention to the effects of nonaxisymmetric gas streams/spirals, which are a dominant feature of hot accretion flows in the MAD regime (e.g., Narayan et al. 2003; Tchekhovskoy et al. 2011; McKinney et al. 2012; White et al. 2019; Chatterjee & Narayan 2022). We follow the GRMHD simulations of McKinney et al. (2012) to set an $R^{-s_{bz}}$ profile of the global vertical component of the magnetic field B_z , where $s_{bz} \approx 1.1$. The field strength is determined by the azimuthally averaged plasma β (gas-to-magnetic pressure ratio) parameter at the outer boundary $200R_g$, i.e., $\bar{\beta}_{z0} = 1.5$ (see Xie & Zdziarski 2019 for the definition of $\bar{\beta}_{z0}$). Other components are calculated numerically according to the gas dynamics, where the magnetic Prandtl number $P_{\rm m}=2$ and a parameter $\kappa_\phi=-0.5$ are

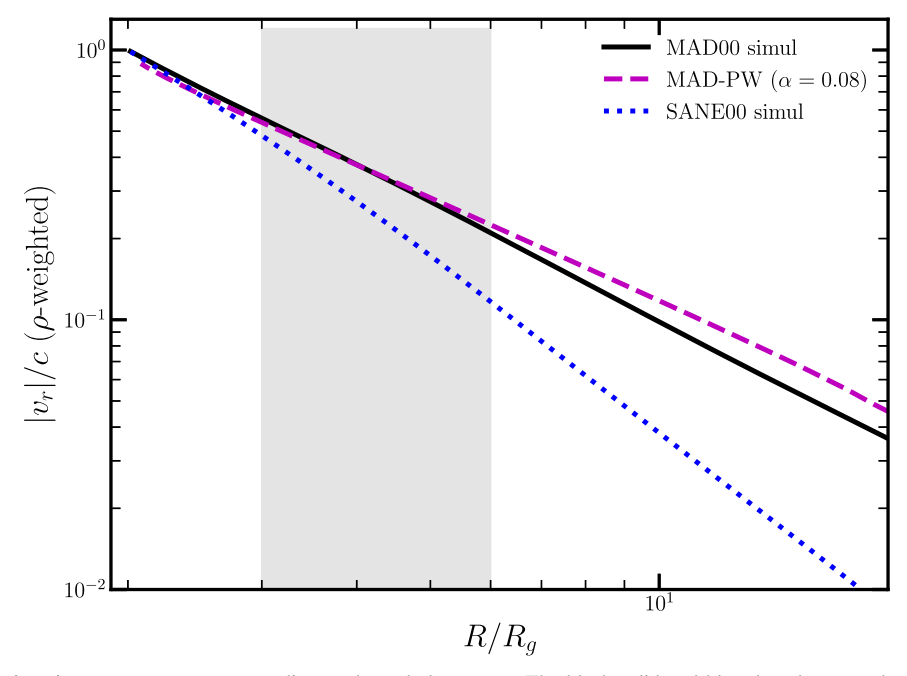


Figure 2. Estimation of the viscosity parameter α corresponding to the turbulent stress. The black solid and blue dotted curves show the density-weighted radial velocity in GRMHD simulations of MAD and SANE models, respectively, around a nonspinning BH (Narayan et al. 2022; Ricarte et al. 2022). The purple dashed curve is derived from our height-integrated MAD model with $\alpha = 0.08$. The shadowed region $(3R_{\rm g} < R < 6R_{\rm g})$ shows where most of the observed radiation comes from.

introduced, respectively, for the calculation of B_r/B_z and B_{ϕ}/B_{z} . With this setup (strength and profile) of global magnetic fields, the vertical magnetic flux threading the accretion flow inside $10 R_g$ is about $50(\dot{M}_{BH}R_g^2c)^{1/2}$, in agreement with that threading the BH in numerical simulations of MAD systems (Tchekhovskoy et al. 2011; McKinney et al. 2012; Davis & Tchekhovskoy 2020; Narayan et al. 2022; see their reported values of the parameter $\phi_{\rm BH}$). The stress of global-ordered magnetic fields, approximately proportional to $B_z B_\phi$ (Xie & Zdziarski 2019), can then be derived. Besides the global field, we also include a turbulent magnetic field by setting the gas-to-turbulent magnetic pressure ratio $\beta_t = 10$. Most importantly, unlike most MHD simulations where a single-fluid equation is adopted, we use separate energy equations for the electrons and ions (Narayan & Yi 1995; Yuan & Narayan 2014; Xie & Zdziarski 2019). As usual, in our model we mimic the turbulent stress term, which is automatically present in MHD simulations, via a radius-independent viscosity parameter α (see Section 3.2 below for the determination of its value).

Numerical simulations suggest that hot accretion flows, including MADs, have a strong mass outflow (e.g., Narayan et al. 2012; Yuan et al. 2012, 2015; Yang et al. 2021) outside of a certain radius $R_{\rm flat}$ (\sim 6–10 $R_{\rm g}$; refer to Figure 5 in Yuan et al. 2015 and Figure 6 in Yang et al. 2021). Inside $R_{\rm flat}$, the outflow is highly suppressed, and the accretion rate is nearly a constant. Instead of the conventional broken power-law fit, we adopt a smooth function for $\dot{M}(R)$, viz, $\dot{M}(R) = \dot{M}_{\rm BH}[1 + (R - R_{\rm BH})^2/R_{\rm flat}^2]^{s/2}$, where s measures the strength of the mass outflow. This expression ensures that $\dot{M}(R) \propto R^s$ for $R \gg R_{\rm flat}$ and $\dot{M}(R) \approx \dot{M}_{\rm BH}$ for $R \ll R_{\rm flat}$. In this work we follow the BH spin a=0 MAD case of Yang et al. (2021) and set $R_{\rm flat} \approx 6R_{\rm g}$, $s \approx 0.2$. Since the outflow strength we adopt is fairly weak (e.g., $\dot{M}(200R_{\rm g}) \approx 2\dot{M}_{\rm BH}$), it has only a minor impact on the radiative efficiency of the model.

3.2. Viscous Parameter α for the Turbulent Stress Term

The "viscous parameter" α (Shakura & Sunyaev 1973), which describes the strength of the turbulent stress, is a free parameter in our model. We note that MHD turbulence can be automatically generated and sustained in MHD simulations of accretion flows (e.g., Stone & Pringle 2001; Igumenshchev et al. 2003; White et al. 2019); thus α is implicitly included there. In our model, α has a strong effect on the predicted radiative output of the model. The radiation emitted by a hot accretion flow is largely determined by the gas density ρ , which, for a given mass accretion rate, is determined by the efficiency of angular momentum transport. The latter is proportional to α in the SANE case (note that in our MAD model the stress by global-ordered magnetic fields is handled separately, based on numerical simulation results; see Section 3.1). For an SANE model, we typically have $\rho \propto \dot{M}_{\rm BH} V_r^{-1} \propto \alpha^{-1} \dot{M}_{\rm BH}$ (Narayan & Yi 1994). A similar expression can also be applied for the magnetic field strength.⁷ In addition, the total dissipated energy is determined by the strength of turbulence, i.e., it is linearly proportional to α in our model; see Xie & Zdziarski (2019). Since part of the dissipated energy goes into electrons (through the δ parameter), the value of α has a direct and strong impact on the radiative luminosity.

As shown in Figure 2, we use the radial velocity measured in a GRMHD MAD simulation (Narayan et al. 2022) of a nonspinning BH to calibrate the value of α in our model. We focus on the region $R \approx (3-6)R_g$ from which most of the observed synchrotron radiation in the EHT band (230 GHz) comes, shown by the shadowed region in Figure 2.

⁷ We note that for the low- $\dot{M}/\dot{M}_{\rm Edd}$ regime appropriate to a hot accretion flow, most radiation is in the form of synchrotron, and for optical depth $\tau \lesssim 10^{-6}$ inverse Compton scattering only plays a negligible role. In this case, the radiative luminosity scales as $L_{\rm bol} \propto \rho B^2 \propto \rho^2 \propto \alpha^{-2} \dot{M}_{\rm BH}^2$ (assuming that the electron temperature is unaffected if $\epsilon \ll 1$; see Narayan et al. 1999 and Figure 1).

The calculated radial profile of the radial velocity as obtained from our height-integrated MAD model with $\alpha=0.08$ is shown as the purple dashed curve in Figure 2. In comparison, the black solid curve shows the velocity profile seen in a long-duration GRMHD MAD simulation with a BH spin a=0 (Narayan et al. 2022). The two profiles agree very well, especially in the shaded region, which produces most of the radiation observed by the EHT. Therefore, we use $\alpha=0.08$ in computing all our model results. For completeness, we also show by the blue dotted curve the GRMHD simulation result for an SANE model with a=0 (Ricarte et al. 2022). There is a large difference, suggesting that the global magnetic field in the MAD model plays an important role in transferring angular momentum and speeding up the radial velocity.

3.3. Radiative Efficiency

We now calculate the radiative efficiency of our height-integrated MAD model using various values of the electron heating fraction parameter δ . As mentioned earlier, there are two sources of heating for electrons in a hot accretion flow: one is through energy transfer from ions via electron–ion Coulomb collisions, and the other is through direct viscous heating at a rate proportional to δ (see Equation (1)). The Coulomb heating rate is $\propto \rho^2$, whereas the viscous heating rate is $\propto \rho$ (e.g., Narayan & Yi 1995). Since $\rho \propto \dot{M}_{\rm BH}$, we expect the impact of δ to be most evident at low values of $\dot{M}_{\rm BH}/\dot{M}_{\rm Edd}$. Thus, among the two sources we are considering, Sgr A* is more likely to give a useful constraint on δ .

For our calculations, we do not focus on detailed microphysics of viscous dissipation (see 1). Instead, we take a "model-independent" approach in which we assume a constant electron heating fraction δ that is independent of radius and explore the observational constraint on its value. We adopt several values: $\delta = 10^{-3}$, 0.1, 0.3, and 0.5. The calculated radiative efficiencies corresponding to these values of δ are shown as a function of $\dot{M}_{\rm BH}/\dot{M}_{\rm Edd}$ in Figure 1. In our calculations, we limit ourselves to the "advection-dominated regime," which corresponds to low accretion rates (Yuan & Narayan 2014). Both M87* and Sgr A* belong to this regime. The maximal accretion rate at the horizon, above which the radiation is so strong that the flow is no longer advection dominated but enters into the "luminous hot accretion flow regime" (Yuan 2001; Yuan & Narayan 2014), is determined numerically by having the advection term $f_{\text{adv}} = 1 - q^{-}/q_{\text{vis}}$ (Narayan & Yi 1994) to be zero at any radius. In our model, this limit is located at $\sim (1-3) \times 10^{-5} \dot{M}_{\rm Edd}$.

Because the strong poloidal field in an MAD system breaks axisymmetry and causes the accretion to occur in the form of dense gas streams surrounded by dilute magnetic voids (Narayan et al. 2003; Tchekhovskoy et al. 2011; McKinney et al. 2012; White et al. 2019; Chatterjee & Narayan 2022), at a given accretion rate, the density of the gas in the accreting streams in an MAD system will be higher than that of the more uniform density in an SANE system. Consequently, the ion–electron Coulomb heating becomes comparable to the turbulent heating at a lower value of $\dot{M}_{\rm BH}/\dot{M}_{\rm Edd}$ in an MAD model compared to an SANE model (compare the results shown in Figure 1 with those in Xie & Yuan 2012).

As seen in Figure 1, the maximal accretion rate of the ADAF regime in MAD models (the upper limits of the curves) decreases with increasing δ . This is naturally expected. At a given accretion rate, a higher δ means a larger fraction of the

viscously dissipated energy goes to electrons. This makes the electrons hotter and radiatively more luminous (higher in radiative cooling q^-). Consequently, it will reach a lower advection term f_{adv} .

In addition, for a typical ADAF regime with $\dot{M}_{\rm BH}/\dot{M}_{\rm Edd} \lesssim 6 \times 10^{-6}$, we find that the radiative efficiency has a roughly linear dependence on the accretion rate: $\epsilon \propto \dot{M}_{\rm BH}^{0.92}$ (for a similar result, see also Xie & Zdziarski 2019). Equivalently, the bolometric luminosity follows $L_{\rm bol} \propto \dot{M}_{\rm BH}^{1.92}$. We note that an estimation of $L_{\rm bol} \propto \dot{M}_{\rm BH}^2$ was derived previously in Narayan et al. (1999) for the SANE case.

We now explore the δ -dependence of ϵ based on our calculations. We find that, at a given accretion rate, the radiative efficiency differs by a factor of \sim 5 for different values of δ . Besides, when $\delta \lesssim 0.05$, the radiative efficiency becomes insensitive to the value of δ because electron heating by Coulomb collisions with ions is dominant. For the typical ADAF accretion rate regime with $\dot{M}_{\rm BH}/\dot{M}_{\rm Edd} \lesssim 6 \times 10^{-6}$, we have $\epsilon \propto \max(\delta^{0.7}, 0.1)$, i.e., $\delta = 0.5$ and $\delta = 0.3$ cases are brighter by a factor of \approx 3 and \approx 2.2, respectively, than the $\delta = 0.1$ case. Combining the dependence on δ and $\dot{M}_{\rm BH}$, our model results can be summarized as

$$\epsilon \approx 1.9\% \left(\frac{\dot{M}_{\rm BH}}{10^{-6} \dot{M}_{\rm Edd}} \right)^{0.92} \max(\delta^{0.7}, 0.1),$$
where $\left(\frac{\dot{M}_{\rm BH}}{10^{-6} \dot{M}_{\rm Edd}} \right) < 6.$ (6)

The dependence of ϵ on δ becomes weaker when $\dot{M}_{\rm BH}/\dot{M}_{\rm Edd}\gtrsim 6\times 10^{-6}$, with $\epsilon\approx (2-4)\%$. This is because of the increasing importance of the Coulomb collision heating of electrons at high accretion rates.

3.4. Constraint on δ from Sgr A* and M87*

Finally, we apply the above theoretical calculations to the observational constraints from Sgr A* and M87*. From Figure 1 we find that in the case of Sgr A*, low values of δ (i.e., δ < 0.3) are ruled out and that $\delta \sim 0.5$ is preferred, given the uncertainties in $\dot{M}_{\rm BH}$. On the other hand, we cannot put any constraint on δ based on the current observational data from M87*. A useful constraint at a similar level to Sgr A* will require the mass accretion rate in M87* to be further constrained to $\dot{M}_{\rm BH}/\dot{M}_{\rm Edd} \lesssim 8 \times 10^{-6}$ (equivalently, $\dot{M}_{\rm BH} \lesssim 10^{-3} M_{\odot} \ \rm yr^{-1}$), i.e., the upper limit on $\dot{M}_{\rm BH}$ will need to be reduced by a factor \sim 2 compared to what the EHT has achieved so far.

4. Summary

In the theory of hot accretion flows around BHs, an important but poorly understood parameter is δ , which describes the fraction of viscous energy that directly heats electrons (refer to Equation (1)). The value of δ determines the thermal energy of electrons and therefore the radiative efficiency of the accretion flow for a given accretion rate. While the underlying microphysics is complicated and the value of δ is poorly determined from theory, in this paper we try to constrain its value by using the most recent EHTC observational and modeling results on M87* and Sgr A*.

The EHTC papers have provided good constraints on the mass accretion rates at the BH horizon for the two sources. These results, combined with the measured bolometric

luminosities of the two objects, lead to useful constraints on the radiative efficiencies, as presented in Equations (3) and (5) and shown in Figure 1. Meanwhile, we can analytically solve the height-integrated dynamical equations of a hot accretion flow in the MAD regime and calculate the theoretically expected radiative efficiency. For this calculation, we need to assume a value for the viscous parameter α . By comparing the radial velocity profile in the height-integrated model with the velocity profile obtained in numerical GRMHD simulations, we estimate that $\alpha \sim 0.08$. Using this α , we calculate the radiative efficiency in our model as a function of the accretion rate and the electron heating fraction parameter δ . By comparing these theoretical results with the observational constraints on Sgr A* and M87* from the EHTC, we are able to estimate the value of δ .

In the case of Sgr A*, we find that we can rule out $\delta \lesssim 0.3$ and that the most likely value is $\delta \sim 0.5$. This result is in excellent agreement with that obtained by Yuan et al. (2003), who modeled the spectral energy distribution of Sgr A*. The analysis in the present paper was made possible because the EHTC reported a tight constraint on the mass accretion rate in Sgr A*. Even if we doubled their uncertainty range, our results would still be largely unchanged. However, we caution that our height-integrated model of MAD accretion makes several approximations whose effects are difficult to quantify.

In the case of M87*, we are unable to obtain a useful constraint on δ because the EHTC does not provide a sufficiently strict constraint on the mass accretion rate.

F.-G.X. is supported in part by National SKA Program of China (No. 2020SKA0110102), the National Natural Science Foundation of China (NSFC; grants 11873074, 12192220, and 12192223), and the Youth Innovation Promotion Association of CAS (Y202064). F.Y. is supported in part by NSFC (grants 12133008, 12192220, and 12192223). R.N. is supported in part by the National Science Foundation under grants OISE-1743747 and AST1816420. R.N.'s work was carried out at the Black Hole Initiative, Harvard University, which is funded by grants from the John Templeton Foundation and the Gordon and Betty Moore Foundation.

ORCID iDs

```
Fu-Guo Xie https://orcid.org/0000-0001-9969-2091
Ramesh Narayan https://orcid.org/0000-0002-1919-2730
Feng Yuan https://orcid.org/0000-0003-3564-6437
```

References

```
Abramowicz, M. A., Chen, X., Kato, S., Lasota, J.-P., & Regev, O. 1995, ApJL, 438, L37

Agol, E. 2000, ApJL, 538, L121

Aitken, D. K., Greaves, J. S., Chrysostomou, A., et al. 2000, ApJL, 534, L173

Algaba, J. C., Anczarski, J., Asada, K., et al. 2021, ApJL, 911, L11

Ball, D., Sironi, L., & Özel, F. 2018, ApJ, 862, 80

Begelman, M. C., Scepi, N., & Dexter, J. 2022, MNRAS, 511, 2040

Bisnovatyi-Kogan, G. S., & Lovelace, R. V. E. 1997, ApJL, 486, L43

Bisnovatyi-Kogan, G. S., & Ruzmaikin, A. A. 1974, Ap&SS, 28, 45

Bisnovatyi-Kogan, G. S., & Ruzmaikin, A. A. 1976, Ap&SS, 42, 401

Blackman, E. G. 1999, MNRAS, 302, 723

Bower, G. C., Dexter, J., Asada, K., et al. 2019, ApJL, 881, L2

Bower, G. C., Wright, M. C. H., Falcke, H., & Backer, D. C. 2003, ApJ, 588, 331

Chatterjee, K., & Narayan, R. 2022, ApJ, 941, 30

Cruz-Osorio, A., Fromm, C. M., Mizuno, Y., et al. 2022, NatAs, 6, 103
```

```
Ding, J., Yuan, F., & Liang, E. 2010, ApJ, 708, 1545
Done, C., Gierliński, M., & Kubota, A. 2007, A&ARv, 15, 1
Dunn, R. J. H., Fender, R. P., Kording, E. G., Belloni, T., & Cabanac, C. 2010,
  MNRAS, 403, 61
Event Horizon Telescope Collaboration, Akiyama, K., Alberdi, A., et al. 2019,
  ApJL, 875, L6
Event Horizon Telescope Collaboration, Akiyama, K., Alberdi, A., et al.
  2022a, ApJL, 930, L16
Event Horizon Telescope Collaboration, Akiyama, K., Alberdi, A., et al.
  2022b, ApJL, 930, L17
Event Horizon Telescope Collaboration, Akiyama, K., Algaba, J. C., et al.
  2021, ApJL, 910, L13
Esin, A. A., McClintock, J. E., & Narayan, R. 1997, ApJ, 489, 865
Gebhardt, K., Adams, J., Richstone, D., et al. 2011, ApJ, 729, 119
Ghisellini, G., Tavecchio, F., Maraschi, L., et al. 2014, Natur, 515, 376
Guo, X., Sironi, L., & Narayan, R. 2017, ApJ, 851, 134
Guo, X., Sironi, L., & Narayan, R. 2018, ApJ, 858, 95
Hada, K., Doi, A., Kino, M., et al. 2011, Natur, 477, 185
Ho, L. C. 2008, ARA&A, 46, 475
Hoshino, M. 2012, PhRvL, 108, 135003
Hoshino, M. 2013, ApJ, 773, 118
Howes, G. G. 2010, MNRAS, 409, L104
Igumenshchev, I. V., Narayan, R., & Abramowicz, M. A. 2003, ApJ, 592, 1042
Kuo, C. Y., Asada, K., Rao, R., et al. 2014, ApJL, 783, L33
Lehe, R., Parrish, I. J., & Quataert, E. 2009, ApJ, 707, 404
Liska, M., Tchekhovskoy, A., & Quataert, E. 2020, MNRAS, 494, 3656
Mahadevan, R., & Quataert, E. 1997, ApJ, 490, 605
McKinney, J. C., Tchekhovskoy, A., & Blandford, R. D. 2012, MNRAS,
  423, 3083
Medvedev, M. V. 2000, ApJ, 541, 811
Narayan, R., Chael, A., Chatterjee, K., et al. 2022, MNRAS, 511, 3795
Narayan, R., Igumenshchev, I. V., & Abramowicz, M. A. 2003, PASJ,
Narayan, R., Mahadevan, R., & Quataert, E. 1999, Theory of Black Hole
   Accretion Disks (Cambridge: Cambridge Univ. Press), 148
Narayan, R., & Yi, I. 1994, ApJL, 428, L13
Narayan, R., & Yi, I. 1995, ApJ, 452, 710
Narayan, R. S., Ädowski, A., Penna, R. F., et al. 2012, MNRAS, 426, 3241
Novikov, I. D., & Thorne, K. S. 1973, in Black Holes, ed. C. DeWitt &
   B. DeWitt (New York: Gordon and Breach), 343
Numata, R., & Loureiro, N. F. 2015, JPIPh, 81, 305810201
Paczyński, B., & Wiita, P. J. 1980, A&A, 88, 23
Prieto, M. A., Fernández-Ontiveros, J. A., Markoff, S., et al. 2016, MNRAS,
  457, 3801
Pringle, J. E. 1981, ARA&A, 19, 137
Quataert, E. 1998, ApJ, 500, 978
Quataert, E., & Gruzinov, A. 1999, ApJ, 520, 248
Quataert, E., & Gruzinov, A. 2000, ApJ, 545, 842
Remillard, R. A., & McClintock, J. E. 2006, ARA&A, 44, 49
Ressler, S. M., Tchekhovskoy, A., Quataert, E., et al. 2015, MNRAS,
  454, 1848
Ricarte, A., Palumbo, D. C. M., Narayan, R., Roelofs, F., & Emami, R. 2022,
   ApJL, 941, L12
Roberts, S. R., Jiang, Y. F., Wang, Q. D., & Ostriker, J. P. 2017, MNRAS,
Rowan, M. E., Sironi, L., & Narayan, R. 2017, ApJ, 850, 29
Rowan, M. E., Sironi, L., & Narayan, R. 2019, ApJ, 873, 2
Ryan, B. R., Ressler, S. M., Dolence, J. C., et al. 2017, ApJL, 844, L24
Shakura, N. I., & Sunyaev, R. A. 1973, A&A, 24, 337
Shapiro, S. L., Lightman, A. P., & Eardley, D. M. 1976, ApJ, 204, 187
Sharma, P., Quataert, E., Hammett, G. W., et al. 2007, ApJ, 667, 714
Sironi, L., & Narayan, R. 2015, ApJ, 800, 88
Stone, J. M., & Pringle, J. E. 2001, MNRAS, 322, 461
Tchekhovskoy, A., Narayan, R., & McKinney, J. C. 2010, ApJ, 711, 50
Tchekhovskoy, A., Narayan, R., & McKinney, J. C. 2011, MNRAS, 418, L79
von Fellenberg, S. D., Gillessen, S., Graciá-Carpio, J., et al. 2018, ApJ,
White, C. J., Stone, J. M., & Quataert, E. 2019, ApJ, 874, 168
Witzel, G., Martinez, G., Hora, J., et al. 2018, ApJ, 863, 15
Xie, F. G., Niedźwiecki, A., Zdziarski, A. A., et al. 2010, MNRAS, 403, 170
Xie, F. G., & Yuan, F. 2012, MNRAS, 427, 1580
Xie, F. G., & Zdziarski, A. A. 2019, ApJ, 887, 167
Yang, H., Yuan, F., Li, H., et al. 2022, arXiv:2206.05661
Yang, H., Yuan, F., Yuan, Y.-F., et al. 2021, ApJ, 914, 131
```

Davis, S. W., & Tchekhovskoy, A. 2020, ARA&A, 58, 407

```
Yuan, F. 2001, MNRAS, 324, 119
Yuan, F., Bu, D., & Wu, M. 2012, ApJ, 761, 130
Yuan, F., Gan, Z., Narayan, R., et al. 2015, ApJ, 804, 101
Yuan, F., & Narayan, R. 2014, ARA&A, 52, 529
```

Yuan, F., Quataert, E., & Narayan, R. 2003, ApJ, 598, 301

Yuan, F., Wang, H., & Yang, H. 2022, ApJ, 924, 124 Zamaninasab, M., Clausen-Brown, E., Savolainen, T., & Tchekhovskoy, A. 2014, Natur, 510, 126

Zdziarski, A. A., Sikora, M., Pjanka, P., & Tchekhovskoy, A. 2015, MNRAS, 451, 927